PCCP



View Article Online **PAPER**



Cite this: Phys. Chem. Chem. Phys., 2024, 26, 23739

High-valent actinyl (AnO₂; An = U, Np and Pu) complexation with TEtraQuinoline (TEQ) ligand a DFT study†

Abigail Jennifer G D and Elumalai Varathan D*

A recently synthesised novel macrocycle composed of four quinoline units called TEtraquinoline (TEQ) (J. Am. Chem. Soc., 2023, 145(4), 2609-2618) was reported to exhibit transition metal complexation ability. Meanwhile, there is a growing interest in different binding motifs for radioactive and toxic actinides. In this study, we modelled high-valent actinyl (AnO₂) $^{n+}$, An = U, Np, Pu; n = 1, 2, 3 complexes of TEQ and studied their geometric and electronic properties using scalar relativistic density functional theory (SR-DFT). The calculated results showed that the equatorial An-N and axial An=O bonds were polar bonds with a high degree of covalence, the former being longer than the latter. Natural bond orbital (NBO) analysis of the An-N bond orders decreased from complexes of uranyl to plutonyl and from complexes of heptavalent to pentavalent actinyls. This was due to the localization of the 5f orbital in the heavier actinyl and the high charge on An. The charge analysis showed a ligand-to-metal charge transfer (LMCT) on complexation. It was interesting to observe metal-to-ligand spin delocalization only in the [AnVIVIIIQ-;LI]2+/3+ complexes, where the spin density on An was observed to increase on complexation. Based on the assigned oxidation states, it was observed that the heptavalent neptunyl cation retained its formal high oxidation state on complexation with TEQ. The energetics associated with the formation reaction of all the actinyl-TEQ complexes suggest spontaneity at lower temperatures (i.e., lower than 298.15 K). The energy decomposition analysis (EDA) indicates that the electrostatic energy contributions were predominant in the $[An^VO_2L]^+$ complexes, while covalent (orbital) energy contributions were higher in the $[An^{VI}O_2L]^{2+}$ and $[An^{VI}O_2L]^{3+}$ complexes. The extended transition state-natural orbitals for chemical valence (ETS-NOCV) analysis confirmed the prominent covalent character in $[An^{VI}O_2L]^{3+}$ over $[An^{VI}O_2L]^{2+}$ and $[An^{VO}O_2L]^{+}$ and the back donation of charges from An to N that stabilizes TEQ.

Received 15th April 2024, Accepted 22nd August 2024

DOI: 10.1039/d4cp01539h

rsc.li/pccp

1. Introduction

Actinyl cations $(AnO_2)^{n+}$, where n = 1, 2, 3, are studied for their unique valence f-orbital characteristics, various accessible high oxidation states (OS) (such as +V, +VI and +VII), and coordination ability with macrocyclic molecules. A clear understanding of their physicochemical properties in non-aqueous media and on complexation is fundamental in developing rational design schemes for ligands that can bind effectively to actinyls. Meanwhile, the presence of these radioactive and toxic heavy metal-based actinyls, commonly in a pool of nuclear waste and in trace amounts in nature (especially, UO₂²⁺), draws attention towards their separation and

Department of Chemistry, SRM Institute of Science and Technology, Kattankulathur 603 203, Tamil Nadu, India. E-mail: varathan.elumalai85@gmail.com

† Electronic supplementary information (ESI) available: Geometric and electronic properties of actinyl cations, cavity size and torsion angles in TEQ before and after complexation, bond angles, O=An=O vibration frequencies, natural bond orders and Mulliken charges in actinyl-TEQ complexes. See DOI: https://doi.org/ 10.1039/d4cp01539h

neutralization from other ionic/free metals and compounds (i.e., of lanthanide and main group metals) before storage or disposal. However, the process of isolating these species poses a challenge given their long-lived radioactive and toxic nature. These fundamental and practical interests in the coordination chemistry of actinyls make the study of their geometric, electronic and bonding properties extremely useful. Actinyl complexes of polypyrrolic macrocycles based on an expanded porphyrin framework are a growing field of interest owing to the ligand's actinyl-compatible cavity size, conformational flexibility, donating ability (mostly through hetero-N atoms) and stability on complexation. 1-9 These ligands are modified based on the number of pyrrole units, nature of linkers, and insertions/replacements of pyrrole with its analogues (such as pyridine, furan, etc.) to enhance their functionality. 10-13

The porphyrin molecule has a planar cavity of 4.103 Å, i.e., the average distance between opposite pyrrolic N atoms, and their complexes with actinides in a 1:1, 1:2 or 2:3 (metal: porphyrin ligand) ratio always results in out-of-plane (single, double or triple-decker, respectively) actinide-porphyrin

Paper

complexes. 14-16 However, the more common expanded porphyrins used in actinide/actinyl complexation studies are known for their larger cavities (i.e., expanded porphyrins have an approximate cavity size of 5.0 Å before complexation; on complexation, the cavity size reduces to 4.8 Å), and conformational flexibility to accommodate the actinide species in the ligand plane (viz., within the ligand cavity). In contrast to the completely pyrrolic expanded porphyrins, modifications that include the more basic pyridine units have drawn attention toward their metalation chemistry, owing to their synthetic feasibility and ability to alter the molecule's chemical behaviours. 17,18 Another pyridine-based analogue - quinoline, has also been used as a heterocyclic substituent in acyclic and macrocyclic ligands for metal complexation study. 19-23 Akhigbe and coworkers had synthesised quinoline-annulated porphyrins, ^{24,25} and utilized the molecule as a ligand for platinum complexation.²⁶ Although the π -conjugation is a sought-after structural feature to increase a ligand's stability and basicity, the steric constraint of quinoline has been a limiting factor towards incorporating these into the skeletal framework of a macrocyclic ligand. Naoya Kumagai and coworkers reported the first quinoline-based pseudo-planar cyclic trimer.²⁷ More recently, they have synthesised TEQ, a saddleshaped four quinoline macrocycle and studied its transition metal complexation ability.²⁸ Despite the lack of planarity, the four N donor atoms and the π -electron conjugation within the quinoline subunits (formed by 10 π -electrons) and the overall extended π -conjugation in TEQ (i.e., 18 π -electron conjugation in porphyrin in comparison with 36 π -electron conjugation in TEO) are desirable features of a metal chelating ligand.

In this study, we employed the DFT method to study the actinyl complexation ability of the tetradentate TEQ macrocycle, shown in Scheme 1. The DFT method has been commonly used to study the physical and chemical properties of actinide/actinyl coordination systems. While the unique global conjugation of the ligand and the donating ability is expected to enhance coordination, the tendency of the ligand to accommodate the actinyl from its twisted configuration is yet to be explored. TEQ is proposed as the smallest four donor macrocycle capable of forming an insertion complex with actinyl. Furthermore, the main objective of this work is to study the actinide-ligand interactions based on their geometric and electronic properties, and to understand the binding affinity and formation feasibilities of these actinyl-TEQ complexes.

2. Computational details

 $(AnO_2)^{n+}$ cations (where, An = U, Np and Pu; n = 1, 2, 3), the TEQ ligand with anisole substitutions (L = TEQ(PhOMe)₂), and $[(AnO_2)^{n+}L]^{n+}$ complexes were modelled and studied through quantum chemical calculations using the DFT method, as implemented in amsterdam density functional (ADF) software.^{29,30} A full unconstrained geometry optimization and frequency calculations were performed. The vibrational frequencies were used to verify that the optimized geometries were the minima on the potential energy surface, and obtain thermodynamic parameters.

Scheme 1 Structure of the TEQ ligand core (top) with notations on heteroatoms and C atoms used to calculate the torsion angle; and TEQ ligand with guinoline substitutions (bottom).

The relativistic effects were accounted for by using the scalar relativistic - zero-order regular approximation (SR-ZORA).³¹ The generalized gradient approximation (GGA) parameterized by Perdew, Burke, and Ernzerhof (PBE)32 was used as the exchange-correlation functional, along with Slater-type orbitals in a triple-ζ plus double polarized (TZ2P) basis set^{33,34} for all calculations. The PBE functional and TZ2P basis sets have been previously used to study macrocyclic actinide-based complexes, and produced comparable results with the experimental observations. 4,11,35-39 Coordination complexes are known to possess van der Waals interactions.40 Hence, we also employed Grimme's dispersion correction (D3)41,42 and Becke and Johnson damping (BJ damping)43 with the GGA:PBE functional (i.e., PBE-D3(BI)/TZ2P) for optimization and calculation of frequencies and energies of all complexes to compare the results of the geometric and energy parameters with those of the pure PBE functional. A frozen core approximation was incorporated to balance the accuracy and computation time. The 1s-4f orbitals were considered frozen in An (An = U, Np and Pu), while the 1s orbital was frozen in C, N and O, and all other electrons were treated variationally. Although neptunyl(vII) is a closed shell moiety, i.e., 5f⁰, all calculations based on neptunyl(vII) were computed with unrestricted spin to verify the actual oxidation state that the actinyl prefers on complexation.

The geometric parameters, including bond lengths and bond angles, were studied from the optimized geometry of the actinyl complexes. The natural bond orbital (NBO 6.0) package implemented in ADF was used to compute the bond orders.44 The natural population analysis (NPA) was carried out to assess the charges and spin density on the individual fragments, i.e., actinyl and TEQ and their complexes. 45 The computed spin densities were used to assign oxidation states to An on complexation, and this was compared to their formal

oxidation state in the respective actinyl cation form. Furthermore, NPA was also carried out using the hybrid: PBE0-D3(BJ) functional (hybrid: PBE0-D3(BJ)/TZ2P//GGA: PBE-D3(BJ)/TZ2P), and the spin densities computed with PBE and PBE0-D3(BJ) were compared. The natural localized molecular orbital (NLMO) analysis helps in understanding the electronic structure of the complex quantitatively through orbital contributions to the molecular orbitals. To account for the nature of interactions between the ligand and the actinide, Bader's quantum theory of atoms in molecules (QTAIM) was computed to analyse the topology based on electron density in the interaction bond path.46,47 The energetics associated with the formation of actinyl-TEO complexes, such as Gibbs free energy (ΔG) , enthalpy (ΔH) , total formation energy (ΔE) , and the temperature and entropy term $(-T\Delta S)$, were calculated using the modelled reaction shown in eqn (1) at a temperature of 298.15 K in the gas-phase. Furthermore, the solvent effect of dichloromethane (DCM), with a dielectric constant of 8.9, was incorporated using a conductor-like screening solvation model (COSMO)⁴⁸ to understand the influence of a bulk solvation environment on complexation. Zero-point energy corrections were included in these energy values, and the default radii for all atoms in COSMO were used, i.e., An, 2.100 Å (An = U, Np, and Pu); C, 1.700 Å; H, 1.350 Å; N, 1.608 Å; and O, 1.517 Å. All calculations were carried out with unrestricted Kohn-Sham formalism to study the open-shell actinyl complexes. The energy decomposition analysis (EDA)⁴⁹⁻⁵¹ was carried out with actinyl as one fragment and TEO as the other, and the attraction and repulsive energy contributions that comprise the actinyl-TEQ interactions were analysed. Apart from PBE and PBE-D3(BJ) functionals, the hybrid: PBE0-D3(BJ) functional was also used for the EDA (based on PBE-D3(BJ) optimized geometries). Furthermore, the extended transition state (ETS) method for EDA combined with the natural orbitals for chemical valence (NOCV) theory was employed to quantify the orbital contributions that suggest the covalent character of the An-TEQ interactions.

3. Results and discussion

3.1. Structure of the TEQ ligand and bare actinyl species

The crystal structure of TEQ was recently synthesised and characterized via X-ray diffraction analysis by Xu and coworkers.²⁸ In this current work, we obtained the initial geometry from CCDC 2202182 reported in ref. 28. The coordinates of the experimentally reported crystal structure were used as the initial input to modify and carry out the geometry optimizations and electronic property calculations of TEQ and their complexes. The optimized geometry of the ligand, along with labelled N donor atoms, is shown in Fig. 1. The bent saddle shape architecture of the quinoline-based core (calculated avg. torsion angle 72.4°) was similar to the structure observed in their single crystal (reported experimental avg. torsion angle 69.2°). The opposite N atoms (i.e., N1 and N3, N2 and N4) were bent away, to the same side, from the horizontal plane of TEQ. The conformation of the molecule was not influenced by anisole

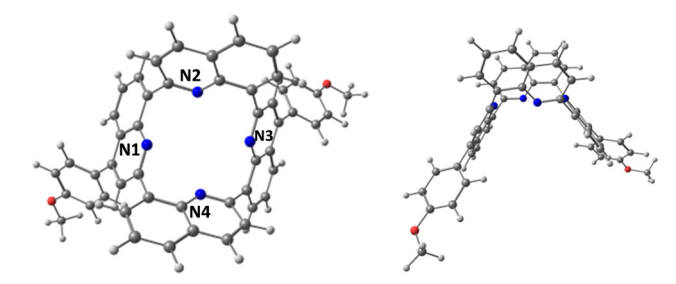


Fig. 1 Top (left) and side (right) views of the optimized structure of TEQ computed at the PBE/TZ2P level of theory in the gas-phase. Carbon – grey, white - hydrogen, red - oxygen, blue - nitrogen.

substitutions at the quinoline units containing N1 and N3. However, it made the molecule chiral. The staggered bonding between the adjacent quinoline units due to steric hindrance results in restricted movement of the units across the single bonds connecting them. The calculated distance between the two quinoline nitrogen atoms is 4.515 Å for N1-N3 and 4.452 Å for N2-N4. This N-N distance (i.e., cavity size) in TEQ is similar to those observed in other pyrrole and pyridine-based macrocycles¹⁰ and larger than that of porphyrin, suggesting that the cavity surrounded by N atoms in TEQ are compatible to fit actinyl cations perpendicular to the ligand plane. The tetradentate ligand was further optimized in the DCE solvent medium to check the influence of an implicit solvation model on its energetics, and thereby its influence on TEQ's complexation feasibility with actinyl.

The geometric properties of dioxo cations (in O=An=O form) of uranium, neptunium and plutonium in +V, +VI and +VII (except U^{+VII}O₂) OS were calculated. The commonly observed highest possible oxidation state in uranium is +VI, as in U+VIO22+. The +VII oxidation state in uranium is not chemically plausible due to a less favourable electronic configuration to achieve the high oxidation state. U at the ground state has [Rn] 5f³ 6d¹ 7s² configuration. In U^{VI+}, there are zero valence electrons, 5f°. Furthermore, to exist at +VII, uranium would need to lose seven electrons and this requires the removal of one inner electron (in addition to all the valence electrons), which would be highly destabilizing, leading to prohibitively high ionization energy. Hence, the combination of a high ionization energy, unfavourable electronic configuration, and lack of sufficient ligand stabilization makes U+VII an impractical oxidation state. Neptunium and plutonium can exist in the +VII oxidation state owing to their electronic configuration, i.e., Np⁷⁺ 5f⁰ and Pu⁷⁺ 5f¹. Based on Hund's rule, the ground state geometry of actinyl cations was assumed to be in their high-spin state configuration, *i.e.*, U⁵⁺ (f¹), U⁶⁺ (f⁰), Np⁵⁺ (f²), Np⁶⁺ (f¹), Np⁷⁺ (f⁰), Pu⁵⁺ (f³), Pu⁶⁺ (f²), and Pu⁷⁺ (f¹). Calculated bond lengths, bond angles, NBO, Mulliken charge and spin density are tabulated in Table S1 (of the ESI†). The linear actinyl cations exhibit a decrease in An=O bond lengths across the series, corresponding to the actinide contraction. The heptavalent species exhibit a significant bend, as observed from their $\angle O = An = O$ (i.e., the avg. $\angle O = An = O$ bond angle in neptunyl and plutonyl is 150.6°). A detailed discussion of the properties of these actinyls is provided in our previous studies.38,39

Paper

3.2. Geometric properties and vibrational frequencies of

actinyl-TEQ complexes

The computationally designed and optimized uranyl(v1) insertion and peripheral isomers, along with their total binding energies of uranyl(v1) - TEQ complex, are shown in Fig. 2. In the peripheral isomer of the [UVIO2L]2+ complex, the uranyl moiety was observed to be bent with $\angle O = U = O = 100.3^{\circ}$, while the corresponding insertion isomer had an almost linear uranyl moiety with $\angle O = U = O = 179.8^{\circ}$. The average equatorial U-N and axial U=O bond lengths were longer by 0.13 Å and 0.03 Å, respectively, in the peripheral isomer (where, the avg. bond lengths of U-N and U=O were 2.517 Å and 1.826 Å, respectively) compared to the insertion isomer (U-N = 2.387 Å and U=O = 1.796 Å). From the figure, it can be observed that the total binding energy of the peripheral isomer is higher (by 13.45 kcal mol⁻¹) than that of the insertion isomer. The more stable insertion isomer with relatively shorter bonds and stronger binding energy between uranyl and TEQ was chosen for further studies of the structure-property relationships and periodic trends. The insertion isomer of the actinyl (V, VI, VII) - TEQ complexes was optimized in the gas-phase, and the geometric and vibrational parameters are displayed in Table 1 and Tables S2-S6 (ESI†). The structures of the optimized complexes are shown in Fig. 3. At the ground state, the spin of the complexes was assigned to be the same as their corresponding actinyl cations. According to Hund's rule, the ground state is characterized by high-spin. The N1-N3 and N2-N4 distance (or the cavity size) in TEQ, shown in Table S2 (ESI†), is observed to increase on complexation. This implies that the cavity expands to accommodate the actinide in the centre with the two oxygen atoms on either side of the ligand (i.e., equatorial) plane. The experimentally observed cavity size of TEQ was 4.5 Å. The computational results showed 4.483 Å and 4.463 Å at PBE and PBE-D3(BJ), respectively. Furthermore, the cavity size of TEQ on

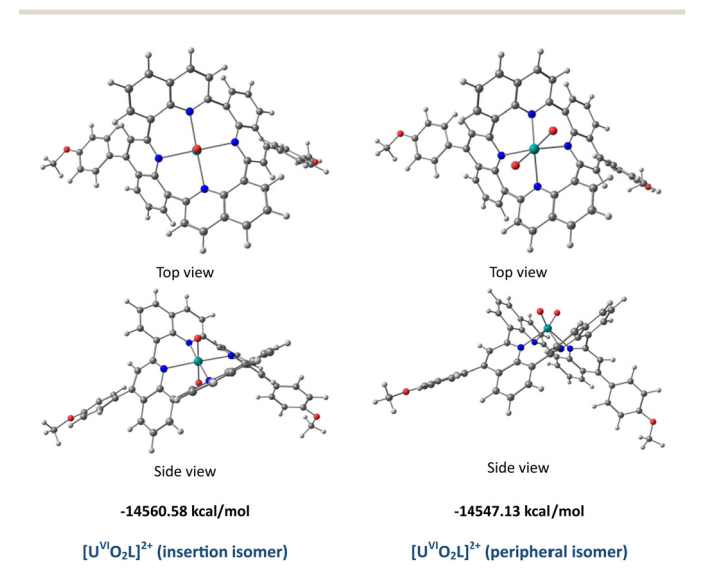


Fig. 2 The insertion and peripheral isomers of the $[U^{VI}O_2L]^{2+}$ complex and their total binding energies computed in the gas-phase at the PBE-D3(BJ)/TZ2P level of theory.

Table 1 Computed bond lengths (in Å) of the actinyl-TEQ complexes in the gas-phase at the PBE/TZ2P level of theory

Complex	An-N1	An-N2	An-N3	An-N4	An=O1	An=O2
$\begin{aligned} & \overline{\left[\text{UO}_2 \text{L} \right]^+} \\ & \left[\text{NpO}_2 \text{L} \right]^+ \\ & \left[\text{PuO}_2 \text{L} \right]^+ \end{aligned}$	2.397	2.419	2.410	2.408	1.814	1.812
	2.407	2.362	2.400	2.456	1.802	1.803
	2.399	2.408	2.403	2.405	1.791	1.788
$\begin{aligned} & \left[\text{UO}_2 \text{L} \right]^{2^+} \\ & \left[\text{NpO}_2 \text{L} \right]^{2^+} \\ & \left[\text{PuO}_2 \text{L} \right]^{2^+} \end{aligned}$	2.374	2.397	2.378	2.397	1.795	1.797
	2.363	2.386	2.365	2.384	1.776	1.778
	2.367	2.366	2.362	2.391	1.764	1.767
$\begin{array}{l} [\mathrm{NpO_2L}]^{3+} \\ [\mathrm{PuO_2L}]^{3+} \end{array}$	2.330	2.361	2.331	2.360	1.770	1.772
	2.366	2.354	2.359	2.372	1.758	1.761

complexation varied between 0.001 Å and 0.010 Å when computed using different functionals like PBE or PBE-D3(BJ). This indicates that the dispersion correction and BJ damping had an almost negligible effect on the cavity size of TEQ. From Table S3 (ESI†), it can be seen that the torsion angles of molecular TEQ decrease from an average of 71° (experimentally reported average torsion angle = 69.2°) on complexation, pointing to the flattened framework acquired on complexation. This is in line with the reported observation, where a decrease in torsion angle was observed in the crystal structure of the FeCl₂ - TEQ complex from the TEQ macrocycle.²⁸ A less significant torsion angle difference was observed between those computed with PBE and PBE-D3(BJ) functionals. The An-N and An=O coordination bond lengths in actinyl-TEQ complexes are tabulated in Table 1 and Table S4 (ESI†). The An-N bond length range observed in these complexes (i.e., 2.360–2.456 Å) corresponds to that reported by Pyykkö (2.37-2.41 Å) as the covalent An-N bond lengths.⁵² This suggests possible covalency in An-N bonding despite being an electrostatic interaction. The An=O bond lengths ranging between 1.758-1.814 Å are much shorter than the An-N bond lengths. They slightly decrease from complexes of U to Pu, and are covalent in nature. The [AnVIIO2L]3+ complexes exhibit shorter bond lengths than the [AnVIO2L]2+ complexes, which in turn exhibit shorter bond lengths compared to their [An^VO₂L]⁺ counterparts. The decrease in ionic radii corresponding to the increase in the assigned oxidation states (from +V to +VII) directly influences (i.e., shortens) the observed bond lengths. All four N atoms of TEQ show nearly similar bond lengths with An pointing to their similar environments, while the anisole substitution to quinoline units with N1 and N3 seems to not affect the TEQ's binding affinities. However, the substitution decreases the ligand's symmetry, making it chiral, while also making it resistant to racemization.²⁸ In [An^VO₂L]⁺ and [An^{VI}O₂L]²⁺ complexes, there is a minor decrease (i.e., of 0.003 Å and 0.007 Å, respectively) in the An-N bond length from uranyl to plutonyl, corresponding to the actinide contraction observed across the actinide series.⁵³ There is an elongation of An=O bonds (by $\sim 0.06 \text{ Å}$) observed on complexation with TEQ, 4,39,54 to accommodate the equatorial coordination with the TEQ ligand. From the functional perspective, i.e., PBE vs. PBE-D3(BJ), a very small difference in An-N and An=O bond lengths was observed, i.e., avg. 0.011 Å. As the bond length difference for suggesting periodic

Published on 22 August 2024. Downloaded on 10/25/2025 9:48:49 PM.

PCCP

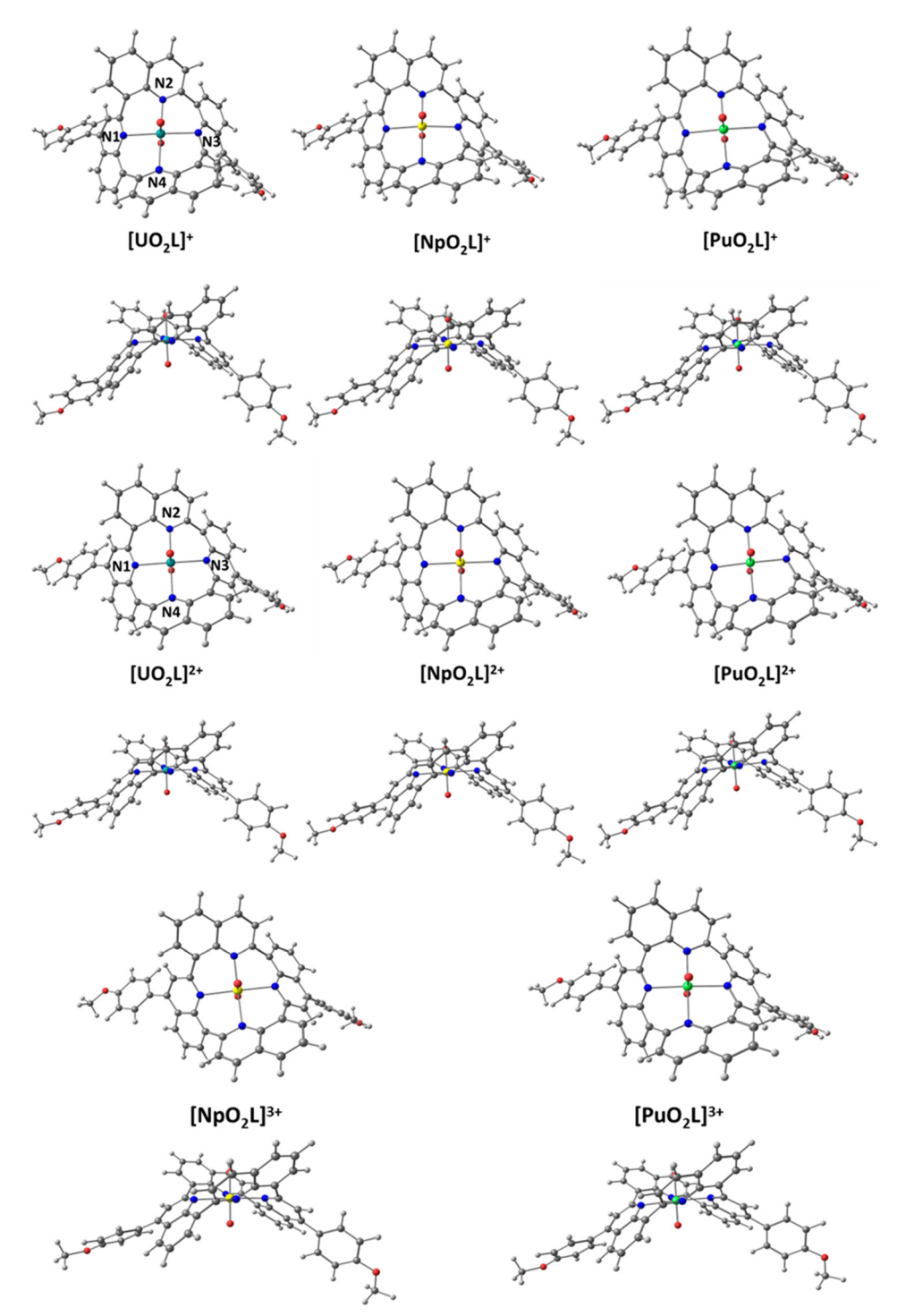


Fig. 3 Optimized geometry of actinyl-TEQ complexes in the gas-phase computed at the PBE/TZ2P level of theory. Carbon - grey, white - hydrogen, red - oxygen, blue - nitrogen, teal - uranium, yellow - neptunium, green - plutonium.

trends between complexes and between An-N, and An=O bonds was around 0.1 and 1.0 Å, respectively, the difference in bond lengths between different functionals is negligible. The bond angles observed in the actinyl-TEQ complexes are tabulated in Table S5 (ESI†). The average $cis \angle N-M-N$ (i.e., adjacent N atoms, *i.e.*, \angle N1-M-N2) is 90°, while the *trans* \angle N-M-N (*i.e.*, opposite N atoms, *i.e.*, ∠N1–M–N3) is 176°, indicating that the

actinide occupies nearly the same plane as the coordinating N atoms of TEQ. A similar coplanarity between the metal and N atoms was observed in the reported TEQ complexes. The O=An=O bond angles in the [AnVVIO2L]+/2+ complexes are nearly the same, and are linear and perpendicular to the ligand plane. It is interesting to note that the significantly bent $(An^{VII}O_2)^{3+}$ actinyl cations (avg. $\angle O = An = O = 150.6^{\circ}$) become

linear (179.7°) on complexation. The steric hindrance of equatorial coordination of the actinide to the ligand pushes the oxygen atoms away from each other, bringing about their linearity.

The calculated vibrational frequencies of actinyls and their complexes are shown in Table S6 (ESI†) and Fig. 4. From the table and figure, we can see that the actinyl O=An=O stretching frequency decreases on complexation due to the competition between the ligand and actinyl oxygen atoms for coordination with the actinide. Shorter bonds exhibit higher vibrational frequencies. The shorter An=O bond lengths in [AnVIIO2L]3+ exhibited higher vibrational frequencies, followed by [AnVIO₂L]²⁺ and [AnVO₂L]⁺. The inverse relationship between the An=O bond lengths and O=An=O vibrational frequencies is consistent. This observation also suggests the possible stabilization of the actinyl species in the TEO environment. Among the actinyl cations, however, we observed (AnO₂)²⁺ with the formal oxidation state of +VI on the actinide to show significantly higher O=An=O stretching frequencies compared to its $(AnO_2)^+$ and (AnO₂)³⁺ counterparts. This suggests stronger binding in the common oxidation of +VI over the others, while pointing to the possible stabilization of the heptavalent actinyl in the common +VI oxidation state. From the table, at the two levels of theories, i.e., PBE and PBE-D3(BJ), the frequencies of the An=O vibrations are observed to lie within a similar range.

3.3. Bond order and natural population charges

The calculated bond order and NPA charges are useful in the analysis of a bonding environment by assessing the nature of interactions and the interacting species. The calculated Mayer bond orders and Wiberg bond index of the An-N and An=O bonds are tabulated in Table 2 and Table S7 (ESI†), respectively. Bond orders show an inverse relationship with bond lengths, such that higher bond orders and shorter bond lengths correspond to better binding. The [AnVIIO2L]3+ complexes show the highest Mayer bond orders for An-N bonds, followed by [AnVIO2L]2+ and [An^VO₂L]⁺. This observation indicates the binding strength to

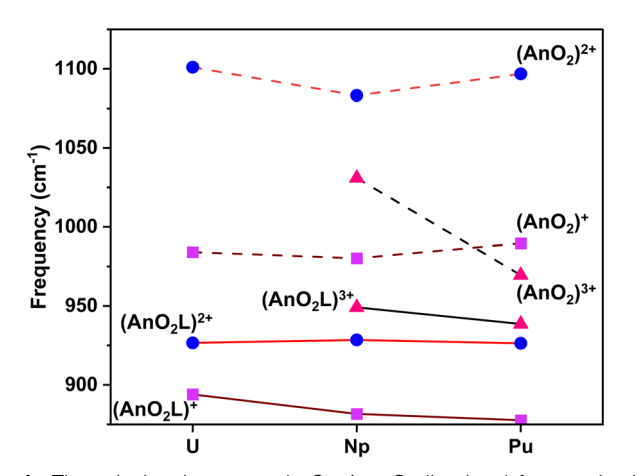


Fig. 4 The calculated asymmetric O=An=O vibrational frequencies in actinyls and their TEQ complexes computed in the gas-phase at the PBE/ TZ2P level of theory.

decrease in the following order: $[An^{VII}O_2L]^{3+} < [An^{VI}O_2L]^{2+} <$ [An^VO₂L]⁺, which aligns with the trend observed from their bond lengths. The charges and the corresponding electronic configuration of An play a vital role in the observed trend. The An=O bonds show higher bond orders than the An-N bonds, indicating a stronger axial interaction of An than its equatorial coordination with TEQ. The higher electronegativity of actinyl's O atoms, compared to that of the N atoms of TEO, is responsible for the formation of polar covalent interactions with An. The An=O and An-N bond orders decrease from U to Pu in their complexes, corresponding to their increasing bond lengths. Anisole-substituted N1 and N3 show slightly higher bond orders compared to N2 and N4, suggesting better interaction of the former N atoms with An compared to the latter. However, the influence of anisole substitution was not observed to affect their bond lengths. From the Wiberg bond orders, it is seen that there is a slight increase (of 0.02) in the An=O bond orders from their pentavalent actinyl cations to their respective TEQ complexes, while a decrease (of 0.10) was observed on going from the hexavalent and heptavalent actinyl's cationic form to their TEQ complexes. The former observation is almost negligible and the increase in An=O bond orders might be a result of electronic stabilization factors, while the latter observation confirms the An=O bond elongation as seen from their bond lengths (i.e., Table 1).

NPA was carried out to study the spin density and charges, including Mulliken charges on atoms of the interacting fragments of the complex. The NPA charges and Mulliken charges on the atoms of the actinyl cations are tabulated in Table S1 (ESI†). The calculated NPA charges and Mulliken charges on the interacting atoms of the actinyl-TEQ complexes are shown in Table 3 and Table S8 (ESI†), respectively. From Table 3, it is observed that all N atoms of the TEQ and actinyl's oxygen atoms have negative charges, indicating the stronger basicity which can be linked to their electronegativities. The higher negative charges on O and their previously observed shorter bond lengths with An, compared to the N atoms of TEQ, can be accounted for the strong covalent character of An=O interactions. Comparing the uranyl-TEQ complex to the plutonyl-TEQ complex, there is a decrease in charges on the An and O atoms. This is due to the poor shielding effect of the 5f electron, resulting in actinide contraction across the series. Hence, the lowered energy 5f orbitals cause less charge transfer in heavier actinides. Such observation is characteristic of actinyl complexes, and has been observed in other actinyl-based complexes. 4,36,39 The NPA

Table 2 The calculated Mayer bond order analysis of actinyl-TEQ complexes in the gas-phase computed at the PBE/TZ2P level of theory

Complex	An-N1	An-N2	An-N3	An-N4	An=O1	An=O2
${\left[\mathrm{UO_{2}L}\right]^{^{+}}}\\ \left[\mathrm{NpO_{2}L}\right]^{^{+}}$	0.387	0.355	0.366	0.365	1.929	1.937
	0.330	0.284	0.351	0.380	1.908	1.918
$[PuO_2L]^+$	0.290	0.279	0.294	0.276	1.905	1.913
$\begin{array}{l} [{\rm UO_2L}]^{2+} \\ [{\rm NpO_2L}]^{2+} \\ [{\rm PuO_2L}]^{2+} \end{array}$	0.372	0.412	0.372	0.423	1.959	1.968
	0.422	0.377	0.428	0.378	1.943	1.955
	0.372	0.329	0.374	0.351	1.934	1.949
$\begin{aligned} & \left[\mathrm{NpO_{2}L} \right]^{3+} \\ & \left[\mathrm{PuO_{2}L} \right]^{3+} \end{aligned}$	0.503	0.434	0.511	0.436	1.949	1.966
	0.379	0.364	0.377	0.383	1.945	1.962

Table 3 Natural population analysis (NPA) of charges on interacting atoms of actinyl-TEQ complexes computed at the PBE/TZ2P level of theory

Complex	An	N1	N2	N3	N4	O1	O2
$\begin{aligned} &\left[\text{UO}_2 \text{L} \right]^+ \\ &\left[\text{NpO}_2 \text{L} \right]^+ \\ &\left[\text{PuO}_2 \text{L} \right]^+ \end{aligned}$	0.920	-0.379	-0.394	-0.398 -0.395 -0.391	-0.395	-0.404	-0.397
$\begin{split} & \left[\mathrm{UO_2L} \right]^{2^+} \\ & \left[\mathrm{NpO_2L} \right]^{2^+} \\ & \left[\mathrm{PuO_2L} \right]^{2^+} \end{split}$	0.921	-0.374	-0.364	-0.373	-0.365	-0.310	-0.301
$\begin{aligned} \left[NpO_2L\right]^{3+} \\ \left[PuO_2L\right]^{3+} \end{aligned}$	0.917 0.825	$-0.352 \\ -0.360$	$-0.358 \\ -0.373$	$-0.351 \\ -0.361$	$-0.358 \\ -0.365$	$-0.255 \\ -0.212$	$-0.243 \\ -0.198$

charges suggest that actinyl(vII) complexes exhibit more quenching of positive charges on An than in corresponding actinyl(v/vi) complexes. The period trends observed in the charges correspond to those observed in their bond properties.

From Tables S1 and S8 (ESI†), the Mulliken charges on An from their actinyl form to the TEQ complex form show a decrease in positive charge. This indicates a charge transfer from the actinyl's O atoms and TEQ's N atoms to the An centre, representing a typical ligand-to-metal charge transfer (LMCT). The average charge on the N atoms in the TEQ molecule was observed to be -0.283e. The charge on the N atoms becomes more negative on complexation, suggesting metal-to-ligand charge delocalization for the stabilization of the individual quinoline rings. It is also interesting to note that the overall charge of the complex is expected to be localized on the An centre. No charge difference was observed between N1/N3 and N2/N4, pointing to the absence of influence of the anisole substitution at the terminals of units containing N1/N3. From Table S8 (ESI†), it can be seen that there is a decrease in charges on the N atoms from uranyl complexes to plutonyl complexes, supporting the observation made from the NPA charges, i.e., a decrease in charge transfer in complexes of heavier actinides. The dioxo ligands of the actinyl fragment in the complexes exhibit more negative charges than in their respective actinyl cation form. This validates the elongation of An=O bonds on complexation, where charges from O → An are shifted closer to O, which is attributed to two reasons. Firstly, the O atom possesses higher electronegativity. Secondly, the repulsion by the equatorial charge contribution N

(of TEQ) → An repels the incoming axial charges on An towards the more electronegative O.

Spin density, orbital population and NLMO

The spin density on the actinyl cations and their complexes are provided in Table S1 (ESI†) and Table 4, respectively. The spin densities and valence orbital population for the actinyl-TEQ complexes were also computed at the hybrid: PBE0-D3(BJ)/TZ2P level of theory, and the results are tabulated in Table S9 (ESI†). From the values, it is observed that the spin density on the An, largely concentrated on its valence 5f orbitals, increases from uranyl to plutonyl. This corresponds to the formal ground state occupancy of the actinyls. On going from [AnVO2L]+ to $[An^{VII}O_2L]^{3+}$, there is a decrease in spin density on the An. This is due to the increase in the formal oxidation state assigned to the An. In $[An^VO_2L]^+$ complexes, the spin density on An is observed to be less compared to that in their corresponding actinyl cation form. This suggests metal-to-ligand spin delocalization in these complexes. This observation supports the previously discussed increase in An=O bond orders, observed in these complexes, suggesting the stabilization of pentavalent actinyl fragments in the TEQ environment through metal-toligand spin delocalization apart from the LMCT. In [AnVIO2L]²⁺ and [AnVIIO2L]3+ complexes, the spin density on An is observed to be higher than in their respective actinyl cations, suggesting ligand-to-metal spin localization. This is supported by the NPA charges which exhibited charge quenching on the An by the axial dioxo ligand (i.e., O atoms) and equatorial TEQ ligand (i.e., through N atoms). The electron spin densities have also been reported as a measure of the oxidation state of the An metal. 55,56 The assigned oxidation state of An based on the spin densities is provided in Table 4 and Table S9 (ESI†). The spin densities computed using the pure GGA showed that U^V, on complexation with TEQ, shifts to the higher and more stable +VI oxidation state. As the spin density is marginal (i.e., 0.443 $(U^{V \to VI})$ in suggesting this shift in oxidation state, the hybrid: PBE0-D3(BJ) functional was employed for verification. The spin density on An, as in Table S9 (ESI†), shows a higher value (i.e., 0.712 (UV)), where the assigned oxidation state is the same as the formal. The 25% of the Hartree-Fock exchange value in the PBE0-D3(BJ) functional contributes to these higher spin density

Table 4 Spin density and orbital population of the actinyl's valence orbital on complexation with TEQ computed through NPA at the PBE/TZ2P level of theory

	NPA spin	density		An's valence orbital occupancy in complex				
Complex	An	Assigned OS	O1/O2 (avg.)	7s	5f	6d	7p	
$\overline{\left[\mathrm{UO_{2}L}\right]^{^{+}}}$	0.443	+V → +VI	-0.018	0.16	3.01	1.53	0.02	
$[\mathrm{NpO_2L}]^+$	1.847	+V	-0.081	0.16	4.36	1.42	0.02	
[PuO ₂ L] ⁺	3.095	+V	-0.146	0.16	5.55	1.36	0.02	
$[\mathrm{UO_2L}]^{2^+}$	0.000	+VI	0.000	0.17	2.92	1.57	0.02	
$[\mathrm{NpO_2L}]^{2^+}$	1.220	+VI	-0.053	0.18	4.26	1.51	0.02	
$[PuO_2L]^{2+}$	2.473	+VI	-0.125	0.18	5.43	1.45	0.02	
$[NpO_2L]_{2}^{3+}$	0.000	+VII	0.000	0.18	4.24	1.56	0.02	
$[PuO_2L]^{3+}$	2.349	$+VII \rightarrow +VI$	-0.119	0.18	5.43	1.47	0.02	

Table 5 NLMOs in the actinyl-TEQ complex observed on An-N bonds computed at the PBE/TZ2P level of theory

Complex	Туре	NLMO
L	LP (N)	94.90% N (32% s/68% p)
$egin{aligned} \left[\mathrm{UO}_2\mathrm{L} ight]^+ \ \left[\mathrm{NpO}_2\mathrm{L} ight]^+ \ \left[\mathrm{PuO}_2\mathrm{L} ight]^+ \end{aligned}$	$egin{aligned} \sigma_{ ext{N-U}} \ \sigma_{ ext{N-Np}} \ \sigma_{ ext{N-Pu}} \end{aligned}$	$\begin{array}{l} 85.9\% \ N \ (sp^{2.65}) + 9.0\% \ U \ (sd^{4.28}f^{2.69}) \\ 86.1\% \ N \ (sp^{2.69}) + 9.4\% \ Np \ (sd^{3.85}f^{2.68}) \\ 86.6\% \ N \ (sp^{2.65}) + 8.6\% \ Pu \ (sd^{3.94}f^{2.60}) \end{array}$
$\begin{split} & \big[\text{UO}_2 \text{L} \big]^{2+} \\ & \big[\text{NpO}_2 \text{L} \big]^{2+} \\ & \big[\text{PuO}_2 \text{L} \big]^{2+} \end{split}$	$\sigma_{ m N-U} \ \sigma_{ m N-Np} \ \sigma_{ m N-Pu}$	$\begin{array}{l} 83.1\% \text{ N } (\text{sp}^{2.78}) + 12.7\% \text{ U } (\text{sd}^{4.28}\text{f}^{4.93}) \\ 81.6\% \text{ N } (\text{sp}^{2.72}) + 14.0\% \text{ Np } (\text{d}^{3.80}\text{f}^{5.95}) \\ 82.5\% \text{ N } (\text{sp}^{2.65}) + 12.5\% \text{ Pu } (\text{d}^{3.86}\text{f}^{5.10}) \end{array}$
$egin{aligned} \left[\mathrm{NpO_2L} ight]^{3+} \ \left[\mathrm{PuO_2L} ight]^{3+} \end{aligned}$	$\sigma_{ m N-Np} \ \sigma_{ m N-Pu}$	80.3% N (sp ^{2.72}) + 15.3% Np (d ^{4.12} f ^{6.72}) 81.0% N (sp ^{2.65}) + 14.3% Pu (d ^{3.88} f ^{5.90})

values. All of the ${\rm An^{VI}}$ -based actinyls retain their formal oxidation state of +VI on complexation with TEQ. It is more interesting to observe the ${\rm Np^{VII}}$ species being stabilized in the TEQ environment, while ${\rm Pu^{VII}}$ shifts to the lower and stable +VI oxidation state. The same observation was made in spin densities computed using PBE and PBE0-D3(BJ). A few other ligand environments have also been previously reported to complex with heptavalent actinyls, retaining their higher oxidation on complexation. 38,57

The natural orbital population of the actinide in its valence orbitals, including 5f, 6d, 7s and 7p, are shown in Table 4. In the complexes, there is a higher degree of occupancy in the 5f orbitals than the 6d orbitals. On complexation, there is an LMCT where the charges primarily enter the 5f orbital of the metal, An. The 5f orbital of An^{VII} in the [An^{VII}O₂L]³⁺ complexes show higher occupancy than their corresponding An^{VI} and An^V in their respective complexes. The 5f and 6d populations increase and decrease, respectively, from uranyl to plutonyl complexes, and this corresponds to the increasing oxidation state assigned to An in the complex. Compared to the valence

orbital population of An^{V/VI/VII} in their actinyl cation form, as shown in Table S1 (ESI†), there is an increase in occupancy (*i.e.*, of 5f, 6d and 7s orbitals) in their corresponding complex form. The ligand-to-metal electron donations can be accounted for in this observation, where the electrons donated by TEQ are mainly accommodated in the 6d and 7s orbitals of An, followed by the 5f orbitals. The stability provided by the common oxidation state of +VI can be accounted for by the increase in occupancy of the valence orbitals of An^{VI} in the complex form compared to its dioxo cationic form. The binding influence of the ligand can be suggested by the population observed on the actinyl. The U^{VI}-based TEQ complex possesses stronger interactions than other actinyl complexes, given the stability induced by the +VI oxidation state and the orbital population of U^{VI} on complexation.

The NLMOs help capture the delocalization associated with the density of the valence electron configuration.⁴⁵ The calculated NLMO results are tabulated in Table 5. The lone pair (LP) of electrons of N atoms of the TEQ ligand are shared by orbital overlap, mainly through their 2p orbitals, with the valence

Table 6 The calculated electron density and energy density parameters at the BCP in actinyl-TEQ complexes computed through QTAIM analysis

QTAIM metrices	Bonds/Complexes	$\left[\mathrm{UO_{2}L}\right]^{\scriptscriptstyle{+}}$	$\left[\mathrm{NpO_{2}L}\right]^{\scriptscriptstyle{+}}$	$\big[\mathrm{PuO}_2\mathrm{L}\big]^{\!\scriptscriptstyle +}$	$[\mathrm{UO_2L}]^{2^+}$	$[\mathrm{NpO_2L}]^{2^+}$	$[\mathrm{PuO_2L}]^{2^+}$	$[\mathrm{NpO_2L}]^{3^+}$	$\left[\mathrm{PuO_{2}L}\right]^{3+}$
Density of all electrons, ρ	An-N1, N3	0.076	0.074	0.073	0.084	0.083	0.081	0.088	0.082
•	An-N2, N4	0.075	0.074	0.072	0.080	0.079	0.078	0.084	0.082
	An=O1, O2	0.274	0.279	0.285	0.288	0.295	0.301	0.306	0.305
Laplacian of electron density, $\nabla^2 \rho$	An-N1, N3	0.200	0.209	0.208	0.195	0.205	0.218	0.239	0.214
	An-N2, N4	0.200	0.208	0.226	0.193	0.200	0.208	0.215	0.205
	An=O1, O2	0.224	0.239	0.262	0.263	0.260	0.270	0.345	0.275
Ellipticity of electron density, ∈	An-N1, N3	0.132	0.160	0.151	0.135	0.129	0.139	0.082	0.132
1 0	An-N2, N4	0.105	0.143	0.079	0.097	0.096	0.101	0.065	0.112
	An=O1, O2	0.013	0.008	0.008	0.010	0.007	0.006	0.017	0.005
Lagrangian kinetic energy, $G(r)$	An-N1, N3	0.072	0.073	0.072	0.079	0.080	0.080	0.090	0.080
	An-N2, N4	0.072	0.073	0.074	0.075	0.075	0.076	0.082	0.078
	An=O1, O2	0.370	0.381	0.398	0.404	0.420	0.433	0.457	0.443
Potential energy density, $V(r)$	An-N1, N3	-0.095	-0.093	-0.091	-0.109	-0.108	-0.105	-0.120	-0.106
3, ()	An-N2, N4	-0.094	-0.093	-0.091	-0.102	-0.101	-0.100	-0.110	-0.105
	An=O1, O2	-0.684	-0.703	-0.730	-0.742	-0.774	-0.798	-0.817	-0.817
Total energy at the BCP $H(r) = V(r) + G(r)$	An-N1, N3	-0.022	-0.020	-0.020	-0.030	-0.028	-0.025	-0.030	-0.026
	An-N2, N4	-0.022	-0.020	-0.017	-0.027	-0.027	-0.024	-0.028	-0.027
	An=O1, O2	-0.314	-0.322	-0.333	-0.338	-0.355	-0.365	-0.374	-0.374

orbitals of the An. The σ interactions between the metal and the ligand through the An-N bonds confirm the covalent coordination interactions that are suggested based on their bond lengths. The distribution at the 5f, 6d and 7s orbitals follows the same trend as observed from their orbital populations. The 6d orbitals are essential in determining the An-L interactions, along with the 5f orbitals. The 5f orbital contribution increases on going from pentavalent actinyl complexes (avg. 2.723) to hexavalent actinyl complexes (avg. 5.326). Finally, the 5f contributions reach the maximum at the heptavalent actinyl complexes (avg. 6.310), while the 6d orbital contributions are nearly the same. On going from uranyl to neptunyl in their TEO complexes, there is an increase in 5f and 6d contributions, and a decrease observed on going from neptunyl to plutonyl-TEO complexes. This can be due to the localization of the 5f orbitals that set in beyond plutonium.

3.5. **QTAIM**

Bader's QTAIM analysis provides more insights into interpreting a chemical bond and the energy partitioning between the interacting atoms based on the topology of the electron density (ρ) . The QTAIM analysis was carried out to study the electron density localized on the centre of the bond paths (i.e., bond critical points, BCP) in the actinyl-TEO complex. The ρ , Laplacian of the electron density $(\nabla^2 \rho)$, ellipticity (\in) , potential energy density (V(r)), kinetic energy density (G(r)) and total energy density (H(r))parameters at BCP of the actinyl-TEQ complexes are shown in Table 6, and the topologies are shown in Fig. S1 (ESI†). Generally, a covalent bond is represented by $\rho > 0.20$ e bohr⁻³ with negative $\nabla^2 \rho$ at BCP, while ionic/electrostatic interactions are represented by $\rho < 0.1 \text{ e bohr}^{-3}$, positive $\nabla^2 \rho$ and H(r) values. Finally, the intermediate type of interaction (such as polar covalent) is represented by positive $\nabla^2 \rho$ and negative H(r). 46,47 The ρ at the BCP of the An=O bonds is higher than that of the An-N bonds, indicating covalent interactions in the former and ionic interactions in the latter. The An=O bonds are polar covalent, as they have positive $\nabla^2 \rho$ and negative H[®], and can also be correlated to their bond orders. These bonds retain their polar covalent character despite their elongation on complexation to accommodate the equatorial TEQ binding. Although An-N bonds are within Pyykkö's An-N covalent bond length range, these interactions have significant electrostatic characteristics.

This is seen from the ρ values of these bonds, while the positive $\nabla^2 \rho$ and negative H(r) at the BCP of the An-N bonds suggest polar covalency in these bonds. This observation indicates that the equatorial bonds have significant characteristics of both electrostatic and covalent interactions. The higher ∈ values of the An-N bonds point to the more asymmetric electron density along the bond path than in the An=O bonds. The non-planar structure and different N atom environments (i.e., substituted (N1/N3) and unsubstituted (N2/N4) quinoline units) of TEQ can account for the higher ∈ values. The distinction between the N atoms of TEQ could not be made based on the ρ , although \in values at the BCP of An-N1/N3 are slightly higher than those of An-N2/N4, indicating the negligible influence of anisole substitution on the binding affinity of coordinating atoms (N1 and N3) and the alteration of the overall complex symmetry density. The ρ , $\nabla^2 \rho$ and H(r) values at the BCPs of An–N and An=O bond paths are higher in [AnVIIO₂L]³⁺ complexes than in [AnVIO₂L]²⁺ and $[An^VO_2L]^+$ complexes, indicating stronger binding in the former. This observation aligns with the discussions based on previous parameters. It is also important to note that the formal charges also influence these observations. There is a slight decrease in electron and energy density parameters going from uranyl to plutonyl complexes of all three oxidation states. This observation is consistent with that observed from their structural and electronic properties. From the figure, it can be seen that ρ is localized closer to the An than N and O atoms, indicating charge quenching on the electropositive An cation by the electron density provided by the donor atoms. On going from uranyl to plutonyl complexes, there is a decrease in ρ at the BCPs of the An-N bonds and an increase in the An=O bonds. The former corresponds to the observation made from their bond lengths, while the latter corresponds to that observed from their bond orders.

3.6. Thermodynamics and energy decomposition analysis

3.6.1. Energetics of formation reaction. Thermodynamic parameters corresponding to the TEQ-actinyl complexation reaction can suggest valuable information on the feasibility and formation energies that would drive the reaction as a lead for experimental investigations. A simple model, based on previous studies, 2,58 for the formation of the actinyl-TEQ complex is as follows:

Calculated thermodynamic parameters (in kcal mol⁻¹) for the formation of actinyl-TEQ complexes computed at the PBE/TZ2P level of theory Table 7

	Gas-phase			DCE medium				
Complex	$\overline{\Delta G}$	ΔH	ΔE	$-T\Delta S$	$\overline{\Delta G}$	ΔH	ΔE	$-T\Delta S$
$[\mathrm{UO_2L}]^+$	-106.09	-119.71	-120.34	13.61	-24.66	-36.06	-37.35	11.40
$[\mathrm{NpO_2L}]^+$	-109.68	-121.62	-123.27	11.93	-36.03	-47.30	-49.03	11.27
$[PuO_2L]^+$	-97.74	-109.51	-111.36	11.77	-23.22	-35.87	-37.22	12.66
$[\mathrm{UO_2L}]^{2^+}$	-277.96	-292.53	-294.54	14.57	-64.07	-77.90	- 79.77	13.83
$[\mathrm{NpO_2L}]^{2+}$	-281.81	-296.53	-298.63	14.72	-75.54	-87.71	-90.23	12.16
$[PuO_2L]^{2+}$	-295.08	-307.20	-309.59	12.11	-102.84	-101.56	-104.04	11.77
$[\mathrm{NpO_2L}]^{3^+}$	-614.58	-628.09	-630.99	13.51	-189.36	-203.63	-205.78	14.27
$[PuO_2L]^{3+}$	-625.67	-640.47	-642.58	14.80	-206.72	-218.92	-221.40	12.20

$$AnO_2^{n+} + L \rightarrow [AnO_2L]^{n+}$$
, where $n = 1, 2, 3$ (1)

The formation reaction based on eqn (1) was computed in the gas-phase, and the energy parameters are tabulated in Table 7 and Table S10 (ESI†). The heptavalent actinyl complexes show the maximum ΔE , followed by hexavalent, and then the pentavalent actinyl-based complexes. This trend is similar to observations made in the bond lengths and bond orders. In heptavalent and hexavalent actinyl-based complexes, the ΔE decreases from the heavier actinyl. Meanwhile, in the pentavalent actinyl complex, the order is as follows: $[Np^VO_2L]^+$ > $[U^VO_2L]^+ > [Pu^VO_2L]^+$. Based on the electronic configuration of Pu^V (i.e., 5f³) and the observed valence orbital population in its actinyl and complex forms, it can be seen that plutonyl(v) has the highest 5f-orbital and lowest 6d-orbital occupancies. It is reported that the 5f-orbital of plutonium is mostly insensitive to different bonding environments.⁵⁹ Hence, the total binding energy is completely dependent on the extent of participation of 6d orbitals, which in this case was observed to be less. This indicates less interaction between the valence orbitals of plutonyl(v) and TEQ, resulting in [PuVO₂L]⁺ with the lowest ΔE value among the pentavalent actinyl complexes. On the other hand, the 6d occupancy in the hexavalent and heptavalent actinyl complexes is observed to be greater than in the pentavalent complexes. The high oxidation state (i.e., +V and +VII) of actinyl and the contracted nature of the 5f and 6d orbitals (i.e., the consequence of actinide contraction) result in a suitable actinyl size that fits TEO's binding cavity. This is validated from the bond lengths and better orbital overlap with that of the ligand's valence orbitals across the actinide series, resulting in the increase of ΔE values from U to Pu complexes. The negative values of ΔG point to the spontaneity of the formation reaction of the actinyl-TEQ complexes, where the positive values of $-T\Delta S$ and negative ΔH values indicate the spontaneity at a lower temperature (i.e., lower than room temperature). The solvation effects play a vital role in replicating a more experimentally relevant environment given the influence of the surroundings on the charges of the interacting species and the formed product. As the experimental synthesis of the FeCl₂-TEQ complexes was carried out in the DCM medium, COSMO calculations using the DCM solvent were used to compute the energetics for the formation reaction, i.e., eqn (1). The calculated solventbased energetics yielded energy values that were less in magnitude. This is due to the environmental effects on the feasibility, while the trends among the complexes and the respective reaction spontaneity remained the same, as observed in the gas-phase calculations. Comparable energies between Table 7 and Table S8 (ESI†) can be observed. This points to the absence of dispersion interactions, which may contribute to non-local correlation effects. The lack of weak intramolecular interactions based on QTAIM analysis and the covalent nature of interactions suggested by geometry parameters validate the comparable energetics calculated at the two levels of theory (i.e., PBE and PBE-D3(BJ)).

3.6.2. EDA and ETS-NOCV. EDA was carried out to quantitatively study the energy contributions that comprise the binding interactions between the actinyl cation and the TEQ ligand

Table 8 EDA analysis of actinyl-TEQ complexes. Actinyl *versus* TEQ, with energy contributions given in kcal mol $^{-1}$ computed in the gas-phase at the PBE/TZ2P level of theory

Fragments	$\Delta E_{ ext{el-stat}}$	$\Delta E_{ m orb}$	$\Delta E_{ m steric}$	$\Delta E_{\mathrm{Pauli}}$	$\Delta E_{ m int}$
$\begin{bmatrix} \mathrm{UO_2} \end{bmatrix}^+ \nu s. \ \mathrm{L} \\ \begin{bmatrix} \mathrm{NpO_2} \end{bmatrix}^+ \nu s. \ \mathrm{L} \\ \begin{bmatrix} \mathrm{PuO_2} \end{bmatrix}^+ \nu s. \ \mathrm{L} \end{bmatrix}$	-223.62 -222.83 -215.66	-188.27 -170.25 -158.25	51.66 38.46 30.72	275.28 261.29 246.38	-136.61 -131.79 -127.53
$\begin{array}{l} \left[\mathrm{UO_2}\right]^{2+} \textit{vs.} \ \mathrm{L} \\ \left[\mathrm{NpO_2}\right]^{2+} \textit{vs.} \ \mathrm{L} \\ \left[\mathrm{PuO_2}\right]^{2+} \textit{vs.} \ \mathrm{L} \end{array}$	-288.13 -288.54 -282.73	-331.79 -322.97 -316.07	5.28 2.96 -4.33	293.42 291.50 278.40	-326.51 -320.01 -320.40
$\left[\mathrm{NpO_2}\right]^{3+}$ vs. L $\left[\mathrm{PuO_2}\right]^{3+}$ vs. L	-359.14 -341.99	$-633.20 \\ -625.88$	-35.68 -49.84	323.46 292.14	-668.88 -675.73

through the An-N bonds. The calculated EDA values are shown in Table 8 and Tables S11, Table S12 (ESI†). AnO2ⁿ⁺ was taken as one fragment and the TEQ ligand as the other, similar to that in eqn (1). From the table, it can be seen that the electrostatic attraction energy ($\Delta E_{\text{el-stat}}$) mainly contributes to the An-L bonding in [AnVO₂L]⁺ complexes. Meanwhile, in the [AnVIO₂L]²⁺ and [AnVIIO2L]3+ complexes, the covalent (orbital) attraction contributions are dominant $(\Delta E_{\rm orb})$ $\Delta E_{ ext{el-stat}}$. This confirms the discussions made based on An-N bond lengths, where the actinyl-TEQ interactions were identified to be covalent in nature and QTAIM analysis. However, the An-N interactions have significant electrostatic contributions. Heptavalent actinyl complexes with shorter bond lengths are seen to exhibit higher $\Delta E_{\rm orb}$ than hexavalent actinyl complexes with relatively longer bond lengths. In [AnVO₂L]⁺ complexes, the dominant $\Delta E_{\text{el-stat}}$ can be attributed to their longer bond lengths, i.e., slightly longer than the Pyykkö's An-N covalent bond length range, and unique metal-to-ligand spin delocalization. On going from uranyl to plutonyl in their complexes, there is a decrease in the $\Delta E_{\text{el-stat}}$, ΔE_{orb} , Pauli's repulsion energy (ΔE_{Pauli}) and total interaction energy ($\Delta E_{\rm int}$), except in the case of $[An^{VII}O_2L]^{3+}$ complexes, where an increase is observed in $\Delta E_{\rm int}$ on going from neptunyl to plutonyl complexes. The [PuVO2L]+ complex has a low ΔE_{int} , while the Pu(+VI, +VII) complexes are observed with higher ΔE_{int} compared to other actinyl complexes in their respective formal oxidation states. This confirms the periodic trend observed in the thermodynamic parameter, ΔE , where plutonyl-(+VI, +VII) complexes exhibited higher ΔE , while plutonyl(+V) complex had the lowest ΔE among other actinyl complexes in their respective formal oxidation states. It is worth noting that the highest possible heptavalent oxidation state of NpVII was retained on complexation, and the complex has high stabilizing energy contributions. On the other hand, the highest energy contributions among all complexes were observed in the PuVII complex (in which Pu was stabilized at an assigned +VI oxidation state on complexation). This indicates that the shift to a lower oxidation state (i.e., +VII \rightarrow +VI in Pu) does not necessarily indicate a reduction of Pu, but rather a redistribution of electron density that stabilizes the plutonyl-TEQ bonding. As seen in the energetics, the EDA energy values computed at the PBE and PBE-D3(BJ) level of theory also show comparable trends across the actinide complexes, confirming the prominent covalent nature of interactions. However, the

dispersion energy ($\Delta E_{\rm disp}$, Table S11, ESI†) contributes an average of -11.32 kcal mol^{-1} to ΔE_{int} of complexes. This ΔE_{disp} is observed to stabilize the complexes by increasing the $\Delta E_{\rm int}$ (by 4 to 6 kcal mol⁻¹), and this is consistent with a previous report.⁴⁰ Furthermore, EDA computed with the hybrid: PBE0-D3(BJ) functional shows a higher magnitude of energy contributions compared to PBE and PBE-D3(BJ) functionals. The PBE0-D3(BJ)-computed values (Table S12, ESI†) show the high values of ΔE_{int} , which increase from heptavalent neptunyl to plutonyl complexes. This is attributed to an increase in ΔE_{orb} and decrease in $\Delta E_{\text{el-stat}}$, while the opposite was observed from the results of the GGA-based functionals.

The results of the ETS-NOCV analysis (Table 9) show the orbital energy component and the dominant deformation

densities. For i = 1, a prominent mix of density inflow and outflow from the actinyl centre can be observed from its deformation density contour. This indicates nearly equivalent contributions to and from the actinyl cation in the complexes, which supports the observation of higher negative NPA charges on N atoms of TEQ in the complexes, pointing to significant back donation from the actinyl to the ligand that stabilized the conjugated ring system. The other dominant deformation densities point to TEQ → An electron donation through both σ bonding interactions between N and An. The energetic stabilization values $(\Delta E_i^{\text{orb}})$ are in the following order: $[An^{VII}O_2L]^{3+} > [An^{VI}O_2L]^{2+} > [An^{V}O_2L]^+,$ which corresponds to the trend observed in previously discussed geometric parameters. There is a decrease in the total ΔE_i^{orb} , *i.e.*, of all *i*, on

Table 9 ETS-NOCV analysis of the orbital energy component (ΔE_i^{orb}) between the actinyl and TEQ, and the corresponding contours of deformation densities (iso-surface value 0.0025) computed at the PBE/TZ2P level of theory

			$\Delta E_i^{ m orb}$ (kcal mol ⁻¹)					
i	Orbital type		U	Np	Pu	Dominant NOCV (([NpO ₂ L] ²⁺) used for representatio		
1	σ	$\begin{aligned} & [AnO_{2}L]^{1+} \\ & [AnO_{2}L]^{2+} \\ & [AnO_{2}L]^{3+} \end{aligned}$	-35.72 -66.94 -	-30.13 -51.76 -125.28	-29.07 -53.67 -148.70			
2	σ	$[AnO_2L]^{1+}$ $[AnO_2L]^{2+}$ $[AnO_2L]^{3+}$	-35.23 -42.16 -	-28.25 -49.47 -105.68	-28.19 -46.02 -106.65			
3	σ	$\begin{aligned} & \left[AnO_2L \right]^{1+} \\ & \left[AnO_2L \right]^{2+} \\ & \left[AnO_2L \right]^{3+} \end{aligned}$	-20.11 -32.97 -	-16.92 -36.21 -84.56	-13.34 -41.00 -78.93			
4	σ	$\begin{aligned} &[AnO_{2}L]^{1^{+}}\\ &[AnO_{2}L]^{2^{+}}\\ &[AnO_{2}L]^{3^{+}} \end{aligned}$	-14.45 -28.02 -	-15.12 -22.22 -61.12	-12.34 -19.09 -48.05			
5	σ	$\begin{aligned} & \left[\text{AnO}_2 \text{L} \right]^{1+} \\ & \left[\text{AnO}_2 \text{L} \right]^{2+} \\ & \left[\text{AnO}_2 \text{L} \right]^{3+} \end{aligned}$	-11.80 -18.05 -	-10.20 -22.04 -31.72	-9.22 -18.53 -24.78			

moving from U to Pu: $[\mathrm{Np^{VII}O_2L}]^{3+}$ (408.4 kcal $\mathrm{mol^{-1}}) > [\mathrm{Pu^{VII}O_2L}]^{3+}$ (407.1 kcal $\mathrm{mol^{-1}}) > [\mathrm{U^{VI}O_2L}]^{2+}$ (188.1 kcal $\mathrm{mol^{-1}}) > [\mathrm{Np^{VI}O_2L}]^{2+}$ (181.7 kcal $\mathrm{mol^{-1}}) > [\mathrm{Pu^{VI}O_2L}]^{2+}$ (178.3 kcal $\mathrm{mol^{-1}}) > [\mathrm{Pu^{V}O_2L}]^{2+}$ (178.3 kcal $\mathrm{mol^{-1}}) > [\mathrm{Pu^{V}O_2L}]^{2+}$ (100.6 kcal $\mathrm{mol^{-1}}) > [\mathrm{Pu^{V}O_2L}]^{+}$ (92.2 kcal $\mathrm{mol^{-1}})$. The higher $\Delta E_i^{\mathrm{orb}}$ values point to better binding between TEQ and the actinyl cation. The trend in $\Delta E_i^{\mathrm{orb}}$ corresponds to that observed in ΔE_{orb} from EDA, suggesting more covalent character in the $[\mathrm{An^{VII}O_2L}]^{3+}$ complexes that decrease across the An series (*i.e.*, U to Pu). However, as discussed based on the EDA results at the PBE0-D3(BJ) level where an increase in ΔE_{orb} of heptavalent actinyl complexes from $\mathrm{Np^{VII}}$ to $\mathrm{Pu^{VII}}$ was observed with an increase in ΔE_{int} , this can be confirmed from the first three major contributions i=1–3, where $\Delta E_i^{\mathrm{orb}}$ is higher in $\mathrm{Pu^{VII}}$ than $\mathrm{Np^{VII}}$ complexes.

4. Conclusions

The new TEQ ligand with two terminal anisole substitutions was studied for its high-valent (+V, +VI and +VII) actinyl (U-Pu) complexation ability using DFT studies. These computationally modelled TEQ-actinyl complexes in their low energy insertion isomeric form exhibited short An=O polar covalent bonds and relatively long An-N coordinate bonds. The bond lengths were observed to slightly decrease across the series, and also on going from heptavalent actinyl-based complexes to pentavalent actinyl-based complexes. These changes were attributed to the decreasing ionic size of the actinides. From the bond orders, it was confirmed that the An=O bonds were stronger and shorter than the An-N bonds. The geometric properties computed with the PBE-D3(BJ) functional showed negligible difference from the PBE-computed values, pointing to the lack of influence of dispersion correction and BJ damping on the geometry of the complex. The bond orders decrease from uranyl to plutonyl in their complexes, indicating decreased binding in the latter due to the localization of 5f-orbitals. N1 and N3, which are closer to the anisole substitutions, showed higher bond orders. However, they have no significant effect on enhancing the binding affinity of TEQ with actinyl ions. The charge distribution suggests LMCT on complexation, while there is significant back donation from the metal to the ligand to stabilize the individual quinoline units, specifically in the pentavalent actinyl-TEQ complexes. The metal-to-ligand back donations are an enhanced stabilizing factor seen in TEQ complexes, owing to its extended π conjugation compared to the porphyrin molecule. The spin density on the interacting atoms of the actinyl-TEQ complex computed through NPA pointed to the metal-to-ligand spin delocalization observed only in the [An^VO₂L]⁺ complexes. The calculated oxidation states using PBE0-D3(BJ) functional indicate that the Np(vII) retained its formal oxidation state on complexation, while the formal Pu(vII) shifted to Pu(vI) on complexation. The latter indicated that the hexavalent oxidation state is a stable high oxidate state. QTAIM analysis showed the electron density at the bond critical points to be closer to the more electropositive An, indicating the quenching of An's cationic charge by the hetero donor atoms (i.e., axial O and equatorial N). Furthermore, the

energetics associated with the complex formation reaction pointed to the spontaneity of the reaction at lower temperatures (i.e., less than 298.15 K), while the DCM solvation decreased the magnitude of the energy values, indicating lowered feasibility caused by charge effects. From the EDA, it was interesting to note that in [AnVO₂L]⁺ complexes, the electrostatic energy contributions were dominant over the orbital energy contributions. Meanwhile, in $[An^{VI}O_2L]^{2+}$ and $[An^{VII}O_2L]^{3+}$ complexes, the orbital energy contributions were dominant and this explains their covalency. The dispersion effects computed at PBE-D3(BJ) stabilized all complexes (around 4-6 kcal mol⁻¹) more than PBE, while the trends among the complexes remained the same. Furthermore, the ETS-NOCV analysis confirms that the significant back donation from the actinyl to the N atoms of TEQ significantly stabilizes TEQ's conjugated framework, and supports the prominent covalent character of the [AnVIIO2L]3+ complexes over the $[An^{VI}O_2L]^{2+}$ and $[An^{V}O_2L]^{+}$ complexes.

Author contributions

A. J. G. – conceptualization, data curation, formal analysis, investigation, validation, visualization, writing – original draft. E. V. – conceptualization, funding acquisition, project administration, software, resources, supervision, validation, visualization, writing – review & editing.

Data availability

The data supporting this article have been included as part of the ESI. \dagger

Conflicts of interest

The authors declare no conflicts of interest.

Acknowledgements

The Science and Engineering Research Board (SERB) provided funding for this study. E. V. would like to express his gratitude to the Department of Science and Technology (DST), SERB for awarding the Startup Research Grant (SERB-SRG) with reference SRG/2022/000207. A. J. G. is grateful for the SRMIST fellowship.

References

- 1 C. Wang, S.-X. Hu, L. Zhang, K. Wang, H.-T. Liu and P. Zhang, Trends in the Electronic Structure and Chemical Bonding of a Series of Porphyrinoid–Uranyl Complexes, *Inorg. Chem.*, 2023, 62(14), 5376–5386, DOI: 10.1021/ acs.inorgchem.2c03986.
- 2 M.-S. Liao, T. Kar and S. Scheiner, Actinyls in Expanded Porphyrin: A Relativistic Density-Functional Study, *J. Phys. Chem. A*, 2004, 108(15), 3056–3063, DOI: 10.1021/jp036927d.

PCCP

3 J. T. Brewster, Q. He, G. Anguera, M. D. Moore, X.-S. Ke, V. M. Lynch and J. L. Sessler, Synthesis and Characterization of a Dipyriamethyrin-Uranyl Complex, Chem. Commun., 2017, 53(36), 4981-4984, DOI: 10.1039/C7CC01674.

- 4 E. Varathan, Y. Gao and G. Schreckenbach, Computational Study of Actinvl Ion Complexation with Dipyriamethyrin Macrocyclic Ligands, J. Phys. Chem. A, 2021, 125(4), 920-932, DOI: 10.1021/acs.jpca.0c08760.
- 5 M. Yang, W. Ding and D. Wang, Characterization of the Binding of Six Actinyls $AnO_2^{2+/+}$ (An = U/Np/Pu) with Three Expanded Porphyrins by Density Functional Theory, New J. Chem., 2017, 41(1), 63-74, DOI: 10.1039/C6NJ01615D.
- 6 J. T. Brewster, H. Zafar, H. D. Root, G. D. Thiabaud and J. L. Sessler, Porphyrinoid f-Element Complexes, Inorg. Chem., 2020, 59(1), 32-47, DOI: 10.1021/acs.inorgchem.9b00884.
- 7 J. L. Sessler, A. E. Vivian, D. Seidel, A. K. Burrell, M. Hoehner, T. D. Mody, A. Gebauer, S. J. Weghorn and V. Lynch, Actinide Expanded Porphyrin Complexes, Coord. Chem. Rev., 2001, 216-217, 411-434, DOI: 10.1016/S0010-8545(00)00395-7.
- 8 J. J. Berard, G. Schreckenbach, P. L. Arnold, D. Patel and J. B. Love, Computational Density Functional Study of Polypyrrolic Macrocycles: Analysis of Actinyl-Oxo to 3d Transition Metal Bonding, Inorg. Chem., 2008, 47(24), 11583-11592, DOI: 10.1021/ic8010772.
- 9 X.-J. Zheng, N. L. Bell, C. J. Stevens, Y.-X. Zhong, G. Schreckenbach, P. L. Arnold, J. B. Love and Q.-J. Pan, Relativistic DFT and Experimental Studies of Mono- and Bis-Actinyl Complexes of an Expanded Schiff-Base Polypyrrole Macrocycle, Dalton Trans., 2016, 45(40), 15910-15921, DOI: 10.1039/C6DT01625A.
- 10 J.-H. Lan, C.-Z. Wang, Q.-Y. Wu, S.-A. Wang, Y.-X. Feng, Y.-L. Zhao, Z.-F. Chai and W.-Q. Shi, A Quasi-Relativistic Density Functional Theory Study of the Actinyl(VI, V) (An = U, Np, Pu) Complexes with a Six-Membered Macrocycle Containing Pyrrole, Pyridine, and Furan Subunits, J. Phys. Chem. A, 2015, 119(34), 9178-9188, DOI: 10.1021/acs.jpca.5b06370.
- 11 G. A. Shamov and G. Schreckenbach, The Role of Peripheral Alkyl Substituents: A Theoretical Study of Substituted and Unsubstituted Uranyl Isoamethyrin Complexes, Inorg. Chem., 2008, 47(3), 805-811, DOI: 10.1021/ic701192t.
- 12 P. Di Pietro and A. Kerridge, Ligand Size Dependence of U-N and U-O Bond Character in a Series of Uranyl Hexaphyrin Complexes: Quantum Chemical Simulation and Density Based Analysis, PhysChemPhys, 2017, 19(11), 7546-7559, DOI: 10.1039/C6CP08783C.
- 13 S. Chattaraj, A. Bhattacharyya and B. Sadhu, Role of O Substitution in Expanded Porphyrins on Uranyl Complexation: Orbitaland Density-Based Analyses, Inorg. Chem., 2021, 60(20), 15351-15363, DOI: 10.1021/acs.inorgchem.1c01981.
- 14 A. Dormond, B. Belkalem and R. Guilard, Unusual Metalloporphyrins: Thorium and Uranium Complexes of Octaethylporphyrin, *Polyhedron*, 1984, 3(1), 107-112, DOI: 10.1016/ S0277-5387(00)84721-X.
- 15 C.-P. Wong and W. De. W. Horrocks, New Metalloporphyrins. Thorium and Yttrium Complexes of Tetraphenylporphin,

- Tetrahedron Lett., 1975, 16(31), 2637-2640, DOI: 10.1016/ S0040-4039(00)75201-4.
- 16 G. I. Vargas-Zúñiga, M. A. Boreen, D. N. Mangel, J. Arnold and J. L. Sessler, Porphyrinoid Actinide Complexes, Chem. 2022, **51**(9), 3735–3758, DOI: **10.1039**/ Soc. Rev., D2CS00107A.
- 17 L. Liu, Z. Hu, F. Zhang, Y. Liu, L. Xu, M. Zhou, T. Tanaka, A. Osuka and J. Song, Benzene- and Pyridine-Incorporated Octaphyrins with Different Coordination Modes toward Two Pd^{II} Centers, Nat. Commun., 2020, 11(1), 6206, DOI: 10.1038/ s41467-020-20072-9.
- 18 J. T. Brewster, D. N. Mangel, A. J. Gaunt, D. P. Saunders, H. Zafar, V. M. Lynch, M. A. Boreen, M. E. Garner, C. A. P. Goodwin, N. S. Settineri, J. Arnold and J. L. Sessler, In-Plane Thorium(IV), Uranium(IV), and Neptunium(IV) Expanded Porphyrin Complexes, J. Am. Chem. Soc., 2019, 141(44), 17867-17874, DOI: 10.1021/jacs.9b09123.
- 19 S. Gaire, R. J. Ortiz, B. R. Schrage, I. B. Lozada, P. Mandapati, A. J. Osinski, D. E. Herbert and C. J. Ziegler, (8-Amino)Quinoline and (4-Amino)Phenanthridine Complexes of Re(CO)₃ Halides, J. Organomet. Chem., 2020, 921, 121338, DOI: 10.1016/j.jorganchem.2020.121338.
- 20 K. Darzinezhad, M. M. Amini, M. Janghouri, E. Mohajerani, M.-R. Fathollahi, Z. Jamshidi and C. Janiak, Introducing Bluish-Green Light-Emitting Diodes (OLEDs) and Tuning Their Color Intensity by Uranium Complexes: Synthesis, Characterization, and Photoluminescence Studies of 8-Hydroxyquinoline Complexes of Uranium, Inorg. Chem., 2020, 59(23), 17028-17037, DOI: 10.1021/acs.inorgchem.0c02242.
- 21 S. Wang, C. Wang, X. Yang, J. Yu, W. Tao, S. Yang, P. Ren, L. Yuan, Z. Chai and W. Shi, Selective Separation of Am(III)/Eu(III) by the QL-DAPhen Ligand under High Acidity: Extraction, Spectroscopy, and Theoretical Calculations, Inorg. Chem., 2021, 60(24), 19110-19119, DOI: 10.1021/acs.inorgchem.1c02916.
- 22 A. N. Carneiro Neto, R. T. Moura, L. D. Carlos, O. L. Malta, M. Sanadar, A. Melchior, E. Kraka, S. Ruggieri, M. Bettinelli and F. Piccinelli, Dynamics of the Energy Transfer Process in Eu(III) Complexes Containing Polydentate Ligands Based on Pyridine, Quinoline, and Isoquinoline as Chromophoric Antennae, *Inorg. Chem.*, 2022, **61**(41), 16333–16346, DOI: 10.1021/acs.inorgchem.2c02330.
- 23 R. M. R. Dumpala, N. Rawat, A. Boda, Sk. M. Ali and B. S. Tomar, Complexation of Thorium with Pyridine Monocarboxylate-N-Oxides: Thermodynamic and Computational Studies, J. Chem. Thermodyn., 2018, 122, 13-22, DOI: 10.1016/j.jct.2018.02.006.
- J. Akhigbe, M. Luciano, M. Zeller and C. Brückner, Monoand Bisquinoline-Annulated Porphyrins from Porphyrin β, β' -Dione Oximes, J. Org. Chem., 2015, **80**(1), 499–511, DOI: 10.1021/jo502511j.
- 25 S. J. Archibald, Coordination Chemistry of Macrocyclic Ligands, Inorg. Chem., 2009, 105, 297, DOI: 10.1039/b818281g.
- 26 J. Akhigbe, M. Luciano, A. O. Atoyebi, S. Jockusch and C. Brückner, Quinoline-Annulated Porphyrin Platinum Complexes as NIR Emitters, J. Porphyrins Phthalocyanines, 2020, 24(01n03), 386-393, DOI: 10.1142/S1088424619501256.

Paper

- 27 S. Adachi, M. Shibasaki and N. Kumagai, TriQuinoline, Nat. Commun., 2019, 10, 3820, DOI: 10.1038/s41467-019-11818-1.
- 28 W. Xu, Y. Nagata and N. Kumagai, TEtraQuinolines: A Missing Link in the Family of Porphyrinoid Macrocycles, J. Am. Chem. Soc., 2023, 145(4), 2609-2618, DOI: 10.1021/ jacs.2c12582.
- 29 E. J. Baerends, T. Ziegler, A. J. Atkins, J. Autschbach, O. Baseggio, D. Bashford, A. Bérces, F. M. Bickelhaupt, C. Bo, P. M. Boerrigter, C. Cappelli, L. Cavallo, C. Daul, D. P. Chong, D. V. Chulhai, L. Deng, R. M. Dickson, J. M. Dieterich, F. Egidi, D. E. Ellis and A. L. Y. Ams, ADF 2019.305, SCM. https://www.scm.com/.
- 30 G. te Velde, F. M. Bickelhaupt, E. J. Baerends, C. Fonseca Guerra, S. J. A. van Gisbergen, J. G. Snijders and T. Ziegler, Chemistry with ADF, J. Comput. Chem., 2001, 22(9), 931-967, DOI: 10.1002/jcc.1056.
- 31 E. van Lenthe, A. Ehlers and E.-J. Baerends, Geometry Optimizations in the Zero Order Regular Approximation for Relativistic Effects, J. Chem. Phys., 1999, 110(18), 8943-8953, DOI: 10.1063/1.478813.
- 32 J. P. Perdew, K. Burke and M. Ernzerhof, Generalized Gradient Approximation Made Simple, Phys. Rev. Lett., 1996, 77(18), 3865-3868, DOI: 10.1103/PhysRevLett.77.3865.
- 33 E. Van Lenthe and E. J. Baerends, Optimized Slater-Type Basis Sets for the Elements 1-118, J. Comput. Chem., 2003, 24(9), 1142-1156, DOI: 10.1002/jcc.10255.
- 34 G. A. Petersson and M. A. Al-Laham, A Complete Basis Set Model Chemistry. II. Open-shell Systems and the Total Energies of the First-row Atoms, J. Chem. Phys., 1991, 94(9), 6081-6090, DOI: 10.1063/1.460447.
- 35 Y. Wang, S.-X. Hu, L. Cheng, C. Liang, X. Yin, H. Zhang, A. Li, D. Sheng, J. Diwu, X. Wang, J. Li, Z. Chai and S. Wang, Stabilization of Plutonium(v) Within a Crown Ether Inclusion Complex, CCS Chem., 2020, 2(4), 425-431, DOI: 10.31635/ccschem.020.202000152.
- 36 S.-X. Hu, W.-L. Li, L. Dong, J. K. Gibson and J. Li, Crown Ether Complexes of Actinyls: A Computational Assessment of AnO₂ (15-Crown-5 $)^{2+}$ (An = U, Np, Pu, Am, Cm), Dalton Trans., 2017, 46(36), 12354-12363, DOI: 10.1039/ C7DT02825C.
- 37 S.-X. Hu, J.-J. Liu, J. K. Gibson and J. Li, Periodic Trends in Actinyl Thio-Crown Ether Complexes, Inorg. Chem., 2018, 57(5), 2899–2907, DOI: 10.1021/acs.inorgchem.7b03277.
- 38 A. Jennifer G, Y. Gao, G. Schreckenbach and E. Varathan, Periodic Trends in the Stabilization of Actinyls in Their Higher Oxidation States Using Pyrrophen Ligands, Inorg. Chem., 2023, 62(18), 6920-6933, DOI: 10.1021/acs.inorgchem.3c00022.
- 39 A. Jennifer G, Y. Gao, G. Schreckenbach and E. Varathan, Chemical Bonding in Actinyl(V/VI) Dipyriamethyrin Complexes for the Actinide Series from Americium to Californium: A Computational Investigation, Dalton Trans., 2022, 51(26), 10006-10019, DOI: 10.1039/D2DT01142E.
- 40 S. K. Singh, C. J. Cramer and L. Gagliardi, Correlating Electronic Structure and Magnetic Anisotropy in Actinide Complexes [An(COT)₂], An^{III/IV} = U, Np, and Pu, *Inorg. Chem.*, 2020, 59(10), 6815-6825, DOI: 10.1021/acs.inorgchem.0c00105.

- 41 S. Grimme and M. Steinmetz, Effects of London Dispersion Correction in Density Functional Theory on the Structures of Organic Molecules in the Gas Phase, PhysChemPhys, 2013, 15(38), 16031, DOI: 10.1039/c3cp52293h.
- 42 S. Grimme, Semiempirical GGA-type Density Functional Constructed with a Long-range Dispersion Correction, J. Comput. Chem., 2006, 27(15), 1787-1799, DOI: 10.1002/ jcc.20495.
- 43 S. Grimme, S. Ehrlich and L. Goerigk, Effect of the Damping Function in Dispersion Corrected Density Functional Theory, J. Comput. Chem., 2011, 32(7), 1456-1465, DOI: 10.1002/ jcc.21759.
- 44 E. D. Glendening, J. K. Badenhoop, A. E. Reed, J. E. Carpenter, J. A. Bohmann, C. M. Morales, C. R. Landis and F. Weinhold, NBO 6.0, Theoretical Chemistry Institute, University of Wisconsin, Madison, Wisconsin, USA, 2001.
- 45 A. E. Reed, R. B. Weinstock and F. Weinhold, Natural Population Analysis, J. Chem. Phys., 1985, 83(2), 735-746, DOI: 10.1063/1.449486.
- 46 R. F. W. Bader, Atoms in Molecules, Acc. Chem. Res., 1985, 18(1), 9-15, DOI: 10.1021/ar00109a003.
- 47 R. F. W. Bader, A Quantum Theory of Molecular Structure and Its Applications, Chem. Rev., 1991, 91(5), 893-928, DOI: 10.1021/cr00005a013.
- 48 A. Klamt and G. Schüürmann, COSMO: A New Approach to Dielectric Screening in Solvents with Explicit Expressions for the Screening Energy and Its Gradient, J. Chem. Soc., Perkin Trans. 2, 1993, 799-805, DOI: 10.1039/P29930000799.
- 49 L. Zhao, M. von Hopffgarten, D. M. Andrada and G. Frenking, Energy Decomposition Analysis, Wiley Interdiscip. Rev.: Comput. Mol. Sci., 2018, 8(3), e1345, DOI: 10.1002/wcms.1345.
- 50 M. Hopffgarten and G. von; Frenking, Energy Decomposition Analysis, Wiley Interdiscip. Rev.: Comput. Mol. Sci., 2012, 2(1), 43-62, DOI: 10.1002/wcms.71.
- 51 K. Morokuma and K. Kitaura, Energy Decomposition Analysis of Molecular Interactions, Chemical Applications of Atomic and Molecular Electrostatic Potentials, Springer US, Boston, MA, 1981, pp. 215-242. , DOI: 10.1007/978-1-4757-9634-6 10.
- 52 P. Pyykkö, Additive Covalent Radii for Single-, Double-, and Triple-Bonded Molecules and Tetrahedrally Bonded Crystals: A Summary, J. Phys. Chem. A, 2015, 119(11), 2326-2337, DOI: 10.1021/jp5065819.
- 53 W. Küchle, M. Dolg and H. Stoll, Ab Initio Study of the Lanthanide and Actinide Contraction, J. Phys. Chem. A, 1997, 101(38), 7128-7133, DOI: 10.1021/jp970920c.
- 54 P. Zhang, Y.-X. Wang, P. Zhang, S.-A. Wang and S.-X. Hu, Evaluation of Chemical Bonding in Actinyl(VI/V) Oxo-Crown-Ether Complexes for Actinide Series from Uranium to Curium, Inorg. Chem., 2020, 59(17), 11953-11961, DOI: 10.1021/acs.inorgchem.0c00535.
- 55 M. P. Kelley, G. J.-P. Deblonde, J. Su, C. H. Booth, R. J. Abergel, E. R. Batista and P. Yang, Bond Covalency and Oxidation State of Actinide Ions Complexed with Therapeutic Chelating Agent

- 3,4,3-LI(1,2-HOPO), Inorg. Chem., 2018, 57(9), 5352-5363, DOI: 10.1021/acs.inorgchem.8b00345.
- 56 M. Vasiliu, T. Jian, J. K. Gibson, K. A. Peterson and D. A. Dixon, A Computational Assessment of Actinide Dioxide Cations AnO_2^{2+} for An = U to Lr: The Limited Stability Range of the Hexavalent Actinyl Moiety, [O=An=O]²⁺, *Inorg. Chem.*, 2020, **59**(7), 4554-4566, DOI: 10.1021/acs.inorgchem.9b03690.
- 57 S.-X. Hu, J. Qin, P. Zhang, M.-B. Shuai and P. Zhang, Theoretical Insight into Coordination Chemistry of Am(v1) and Am(v) with Phenanthroline Ligand: Implications for High Oxidation State Based Minor Actinide Separation,
- Inorg. Chem., 2020, 59(9), 6338-6350, DOI: 10.1021/ acs.inorgchem.0c00452.
- 58 Z. Szabo, T. Toraishi, V. Vallet and I. Grenthe, Solution Coordination Chemistry of Actinides: Thermodynamics, Structure and Reaction Mechanisms, Coord. Chem. Rev., 2006, 250(7-8), 784-815, DOI: 10.1016/j.ccr.2005.10.005.
- 59 T. Vitova, I. Pidchenko, D. Fellhauer, P. S. Bagus, Y. Joly, T. Pruessmann, S. Bahl, E. Gonzalez-Robles, J. Rothe, M. Altmaier, M. A. Denecke and H. Geckeis, The Role of the 5f Valence Orbitals of Early Actinides in Chemical Bonding, Nat. Commun., 2017, 8(1), 16053, DOI: 10.1038/ ncomms16053.